Dissimilar Friction Stir Welds in AA5083-AA6082. Part II: Process Parameter Effects on Microstructure

M.J. PEEL, A. STEUWER, and P.J. WITHERS

The aim of this study is to explore the bounds of the so-called processing window, within which good-quality welds can be produced, for the friction stir welding of AA5083 to AA6082 using a systematic set of rotation and traverse speeds. The first paper in this series examined the thermal and macroscopic aspects. In this paper, several microstructurally related characteristics, including hardness, grain size, and precipitate distribution, have been examined in greater detail. The observed variations are correlated and contrasted with the observed and predicted thermal distributions. In addition, the thermal model developed in part I has been coupled to hardness models based on classical isothermal aging studies for each alloy to predict the hardness variations across the welds.

I. INTRODUCTION

AS a relatively new joining technique,[1] few systematic studies of friction stir (FS) welding have been performed. The relationships between the various weld parameters and the resulting weld properties have not been identified, and there are many remaining questions. The aim of this study is to investigate the bounds of the so-called processing window—the range of welding speeds (rotation and traverse) within which good-quality welds will be produced—for the FS welding of AA5083 to AA6082.

In part I,[2] the impact of changes in the rotation and traverse speed on the global process parameters (forces, torque, and power input) and the thermal excursion and macrostructure were determined. A thermal model was presented that was calibrated against thermocouple data in the weldments and in the supporting backing plate. This model indicated that the temperature under the tool is more strongly dependent on the rotation speed than the traverse speed. This conclusion was supported by the measured torque data and the extent of material flow around the tool. In this paper, the microstructure and local mechanical properties are examined in greater detail. In addition, the outputs of the thermal model are coupled to analytic models for predicting the hardness variation of the two alloys across the dissimilar welds to elucidate the relationship between the welding parameters and the subsequent weld properties.

The variation in hardness in welded AA6xxx aluminum alloy series has been previously linked with changes in the precipitate distribution due to the imposed thermal cycle.[3,4,5] Far from the weld line, the lower temperatures cause the β'' precipitates to coarsen or transform to the nonhardening β' phase, reducing the hardness. At higher temperatures the precipitates dissolve, with the reverted fraction increasing as one nears the weld line. During cooling, some of this solute may reprecipitate as stable, nonhardening phases such as β'. The remaining solute results in some strength recovery via natural aging in the days and weeks following welding.

M.J. PEEL, Post-Doctoral Fellow, A. STEUWER, Post-Doctoral Fellow, and P.J. WITHERS, Professor, are with the Materials Science Centre, Manchester University, Manchester, U.K. M.J. PEEL and A. STEUWER are with FaME38 at the ESRF-ILL, Grenoble, France. Contact e-mail: peel@ill.fr

Manuscript submitted September 29, 2005.

The AA5xxx series of alloys may be used in the annealed or strain hardened condition. If the alloy has been annealed, then the microstructure is stable and no softening will occur in the heat-affected zone (HAZ). In contrast, a worked structure will readily recover or recrystallize during welding, so softening may occur.[6] The AA5083 material used in the current study is in a highly cold-worked condition, and the welding process has been shown to result in significant softening through recovery and recrystallization.[7]

II. EXPERIMENTAL PROCEDURE

Two materials form the basis of this study: AA5083 (cold-rolled) and AA 6083 (peak-aged) (see Table I in part I). As described in part I,[2] these were welded at three rotation speeds (280, 560, and 840 rpm) and three traverse speeds (100, 200, and 300 mm), with the AA5083 alternately placed on the advancing and retreating sides of the welds to form a set of 18 welds labeled M1-9 and M11-18 (Table II of part I). The welding tool had a shoulder of 18-mm diameter and a 6-mm M6 pin. Electron backscattered diffraction (EBSD) and conventional scanning electronic microscopy (SEM) analysis were performed on a PHILIPS*

*PHILIPS is a trademark of FEI Company, Hillsboro, Oregon.

XL30 field emission gun (FEG) SEM fitted with a Channel EBSD system (HKL Technology, Denmark). Samples were prepared using conventional grinding and polishing methods, with an additional electropolishing step in a mixture of 30 pct nitric acid in methanol, cooled to −30 °C by liquid nitrogen, for 20 to 30 seconds at 12V. All electron microscope images were taken on the normal-transverse (NT) cross-section. The microscope was operated at 20 KeV and the sample was tilted by 70 deg to the electron beam axis. The maps were up to 200 × 150 μm in size and used a step size of 0.5 μm. Such a map requires around 120,000 points and takes around 30 to 40 minutes to collect using the current set-up. Subsequent EBSD data analysis and presentation were carried out using the VMAP software.[8] A high-angle grain boundary was defined as having a misorientation greater than 15 deg, while a low-angle boundary had a range of 1.5 deg to 15 deg. Grain size measurements were performed using the linear intercept method

Table I. Values Used by Myer and Grong for the Natural Aging Response of AA6082

Parameter	Definition	Value
A_0	Material constant for nucleation of β' (Mg_sSi)	3.6 10^8 J K^2/mol
Q_d	Activation energy for Mg diffusion in Al	130 KJ/mol
T_s	β' phase boundary solvus	520 °C
T_{r2}	Reference temperature	350 °C
$t^*_{r_2}$	Time required to precipitate arbitrary fraction of β' at T_{r2}	3 secs

and neglecting the low-angle boundaries. In the majority of cases 200 to 1,000 grains were sampled, which is generally considered sufficient to provide adequate statistics.[9]

TEM examination took place in a Philips EM400T operating at 120 KeV with a two-axis sample mount. A series of thin NT sections were cut from the welded plate. Typical dimensions were 50 mm (transverse) × 1 mm (longitudinal) × 3 mm (thickness). These sections were then attached to a metal block and gently ground using fine SiC until they were 0.2 mm thick. Three-millimeter disks were then punched out from the required locations. Further thickness reduction (~100 nm) was achieved by grinding the samples on 1200-grade SiC paper using a purpose-made mount. Final polishing was performed on a Struers electro-jet polisher using a 30 pct nitric acid in methanol mixture and operating in automatic (light sensing) mode with a potential of 30V.

Hardness testing was performed on the NT plane at the midthickness of the plate using a single line of indents. Indentation was performed using a TUKON* microhardness indenter. A 1-kg load was used, corresponding to indents that were typically 80 to 110 μm along the diagonal axis. Tests on nonwelded material had a standard deviation of around 2 HV. Hardness testing took place over 4 weeks after welding, so any postweld natural aging would have been substantially complete.[10]

*TUKON is a trademark of Wilson Instruments, Norwood, MA.

To characterize the thermal response, isothermal heat treatments were performed on small test pieces (20 × 15 × 3 mm) cut from plates of unwelded parent material. These were removed from the parent plate in such a way as to ensure that the hardness could be measured on the same plane as the NT cross-section in the welds (*i.e.,* the indenter axis is parallel to the rolling direction in the plate). These were then immersed in a salt bath at a temperature between 250 °C and 525 °C. The temperature of the salt bath was determined by a *k*-type thermocouple suspended at the same height as the immersion depth of the samples. The immersion time was between 3 and 3,000 seconds, and the samples were water-quenched within 1 second of leaving the bath. The AA6082 samples were hardness-tested using 5 to 10 indents within 10 minutes of quenching to minimize the effect of natural aging. The recovery of strength by natural aging was evaluated by retesting the AA6082 samples 6 weeks after the heat treatment.

III. RESULTS

A. *Effect of Process Parameters on Hardness Distribution*

The variation in hardness with (a) traverse speed at fixed rotation speed, (b) rotation speed at fixed traverse speed, and (c) increasing speeds at constant weld pitch are shown in Figure 1 for the dissimilar welds with AA5083 on the advancing side. In addition, the results for welds M1, M3, M7, and M9 have been plotted together to allow a direct comparison of the hardness profiles for the welds produced at the corners of the parameter matrix (Figure 2). Although the tool dimensions are shown for reference inset in each figure, this does not necessarily correspond to their field of influence.

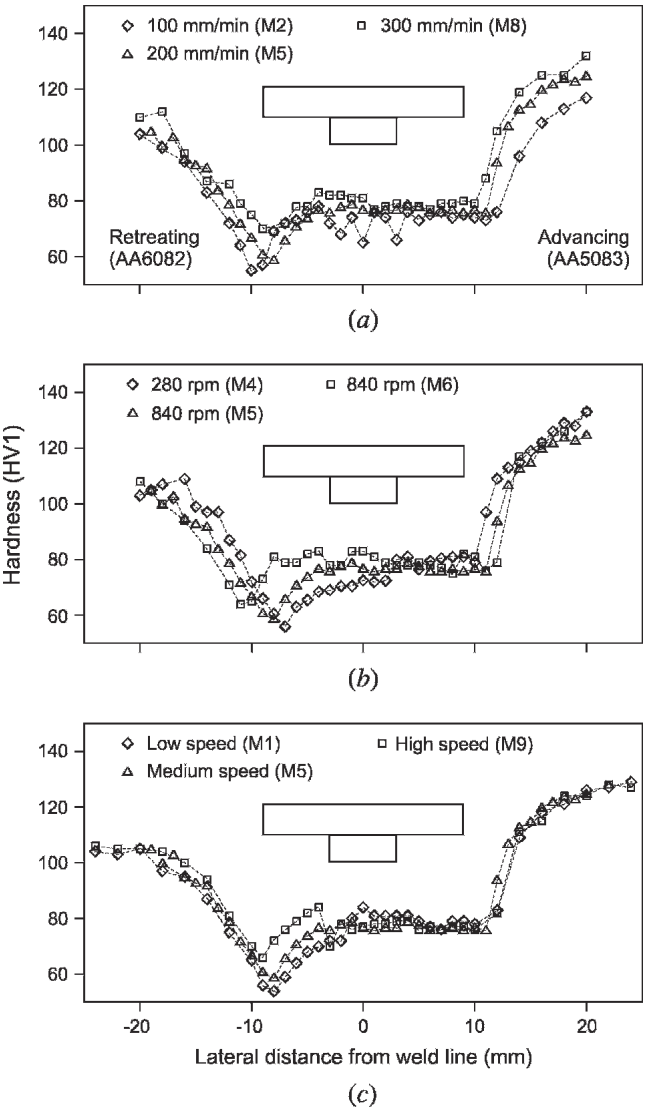

Fig. 1—Variation in hardness across dissimilar FS welds produced at (*a*) constant rotation speed (560 rpm), (*b*) constant traverse speed (200 mm/min), and (*c*) constant weld pitch (0.36 mm/rev) but steadily increasing speed (standard deviation ~2 HV).

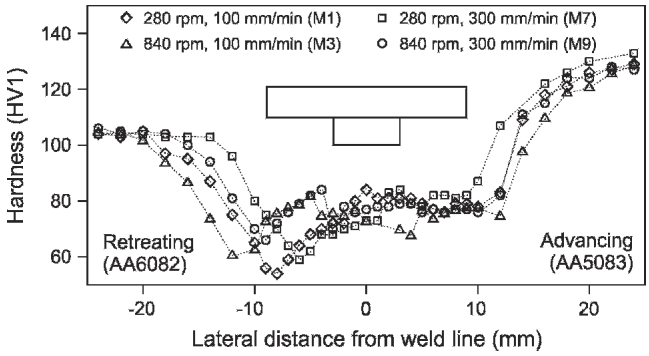

Fig. 2—The variation in hardness across dissimilar AA6082–AA5083 FS welds produced at the extremes of the weld process parameter matrix (standard deviation ~2 HV).

1. *AA5083 response*

The hardness variations in the AA5083 show good agreement with those seen for the similar AA5083-AA5083 welds analyzed previously, where the softening behavior has been attributed to the recovery and recrystallization of the heavily cold-worked microstructure.[7] The first evidence of significant material softening can be seen around 20 to 25 mm from the weld line, with the hardness decreasing rapidly as one approaches the weld line to reach a somewhat steady state value of ~78 HV. There is some evidence of a very slight increase in the hardness in the welds produced at low rotation speed and/or high traverse speed (M4, M8, and M7). In these welds the hardness tends to be around 5 HV higher than in the other welds. Within the stir zone the scatter in the hardness increases noticeably, possibly as a result of the material mixing, and it is difficult to observe any systematic difference in the hardness between the different welds. It can be seen that either increasing the rotation speed or decreasing the traverse speed results in a wider HAZ, presumably as a result of the greater heat input. At constant weld pitch (*i.e.,* welds M1, M5 and M9), the hardness profiles are essentially the same, suggesting a similar thermal profile in the HAZ. The transition region between the unaffected parent material and the hardness plateau is fairly narrow, generally being around 10 mm wide.

2. *AA6082 response*

The variation in hardness within the AA6082 material on the retreating side is complicated by the over-aging or dissolution of the hardening precipitates, combined with the subsequent potential for natural aging. Upon approaching the weld line, softening is first noticeable between 14 to 23 mm from the weld line (depending on the welding speeds); the hardness reaches a minimum (typically around 60 HV) between 6 and 13 mm from the weld line and increases again in and around the stir zone. This corresponds to the location of failure in cross-weld testing (see part I).

Changes in the welding parameters have the following effects on the AA6082 response: *Traverse speed* (Figure 1(a)): As the traverse speed is increased, the minimum hardness increases slightly and forms closer to the weld line. This is consistent with a lower temperature and a briefer thermal cycle. Such variations have been predicted in this alloy for fusion welding processes.[11,12] *Rotation speed* (Figure 1(b)): The change in hardness as the rotation speed increases is more complicated than for the traverse speed. The hardness minimum moves further from the weld line as the rotation rate increases, which is consistent with an increase in the heat input as observed in part I.[2] Somewhat surprisingly, the minimum hardness actually increases when the rotation speed is increased. An increase in temperature might be expected to result in more extensive overaging and hence a lower hardness, and *Constant weld pitch* (Figure 1(c)): As the weld is approached, the softening behavior is similar irrespective of the welding speeds until the hardness minimum is reached. In contrast, close to the tool the extent of natural aging is strongly influenced by the change in tool speed and is greater for the welds produced at high speeds. This suggests that the dissolution and overaging kinetics have a different response to changes in the peak temperature and the length of the thermal cycle. Specifically, high temperatures and rapid thermal cycles appear to encourage dissolution and the retention of solute in the matrix, with subsequently increased natural aging, at the expense of coarsening or the reprecipitation of nonhardening phases during cooling. As a result, and unlike the AA5083 material, the weld pitch is not such a useful qualifying parameter for the hardness variation in the AA6082 sides of the welds.

B. *Precipitate Distribution*

The variation in precipitate microstructure for AA6082 is shown in Figure 3. Those in Figures 3(b) and (c) are located approximately at the position of minimum hardness. In the parent plate (Figure 3(a)), there is a significant density of needle-shaped precipitates, aligned along the {001} axis, having typical dimensions of $\sim 20 \times 5 \times 5$ nm. The morphology and dimensions of these particles are consistent with the β''-phase discussed in the literature.[13,14] As anticipated, in the region of minimum hardness it can be seen that the precipitates have over-aged significantly, being several times larger than in the parent plate. They have retained the needle- or rod-like morphology and remain aligned to the {001} axis. These precipitates are typically over 100 nm in length and are most probably β' precipitates.[15] It was not possible to resolve any precipitates in the region close to the tool. This is not surprising, given that the TEM used does not have a sufficient resolution to resolve GP zones. The thermal stability of the larger (~ 1 μm) Al_6Mn particles means that these are still observed (qualitative EDX confirmed their composition). The grains also contained a greater number of dislocations compared to those further from the weld line. This is presumably an indication of deformation by the tool in this region. These results are consistent with the TEM analysis performed by Svensson *et al.* in a nominally identical alloy.[5]

C. *Distribution of Grain Structure*

The variation in grain structure across the welds is typified by that for M5 shown in Figure 4. In the AA6082 material the passage of the tool results in the deformation of the original grains in the thermomechanically affected zone (TMAZ). This deformation is accompanied by an increased fraction of low-angle grain boundaries (35 to 40 pct of total boundary length compared to <5 pct in the parent plate). In agreement with the literature,[16,17]

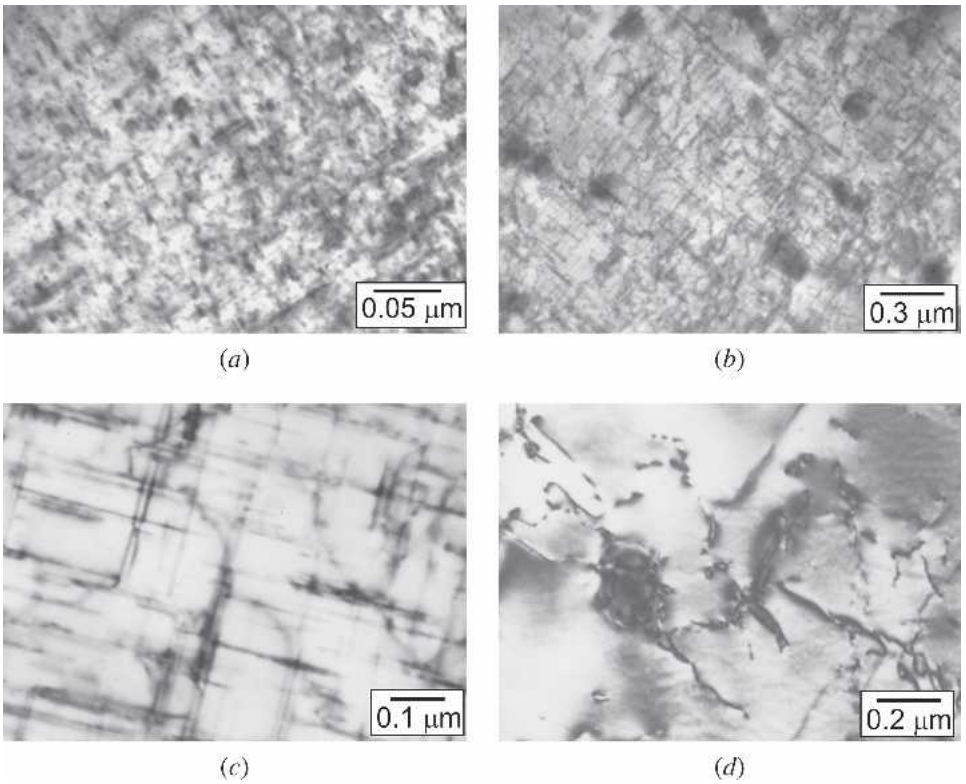

Fig. 3—TEM micrographs for AA6082: (*a*) parent plate, (*b*) the HAZ of weld M3 (12 mm from the weld line), (*c*) as (*b*) but higher magnification, and (*d*) 6 mm from the weld line in the fully reverted and naturally aged region.

the strain appears to have been insufficient to bring about significant recrystallization. Due to the size of the grains in this material, it was not possible to produce statistically relevant grain size data.

In contrast to the AA6082 material, the microstructure in the AA5083 appears to be essentially independent of distance from the tool within the low hardness plateau. The mean linear intercept (MLI) of the grains is 5.79 ± 0.8 μm at 0 mm, 6.11 ± 0.6 μm at 5 mm from the weld line, and 6.12 ± 1.1 μm at the edge of the tool shoulder (8 mm). A grain size of 6.85 ± 0.3 μm was recorded beyond the shoulder at 10 mm (not shown). In all cases, the fraction of low-angle boundaries is also constant at around 20 pct, which is rather less than in the AA6082 material. The lack of variation in the grain size with distance from the tool would suggest that because the parent plate was in the cold-worked condition, there is sufficient driving force for recrystallization within the hot zone beneath the shoulder, irrespective of the deformation caused by the pin. As a result, the grain size is likely to be determined primarily by the temperature around the tool, with lower temperatures producing a smaller grain size.[18] This is confirmed by our finding that while the grain size shows a strong dependence on the processing conditions (Figures 5 and 6), it is essentially constant within the region characterized by the plateau of low hardness.

The striking relationship between process conditions and the grain size in the process zone of the AA5083 is evident from Figures 5 and 6. It is clear from both figures that the grain size decreases as the traverse speed increases or the rotation speed decreases (*i.e.,* as the weld pitch increases). Consequently, the grain size is the largest for weld M3 (8.5 μm) and smallest for weld M7 (2.5 μm). Generally speaking, the rotation speed appears to have a more significant effect on the grain size than the traverse speed; as a result, using a faster rotation speed while maintaining the weld pitch will result in a larger grain size. This is consistent with the temperature predictions presented in part I.[2]

D. *Hardness Response to Isothermal Exposure*

To understand the variation in hardness across the FS welds, a series of hardness measurements were carried out on samples isothermally exposed to different temperatures. The effects of hold time at several temperatures on the hardness of the AA5083 parent material are summarized in Figure 7(a). As would be expected, the rate of softening increases considerably as the annealing temperature is increased. Indeed, above 345 °C it was not possible to determine the kinetics, as the material had fully softened in less than 3 seconds (the minimum practical test time).

The effect of isothermal hold time on the hardness is shown in Figure 8(a) for several isothermal temperatures. These values were all determined within 10 minutes of quenching (the minimum practical time) to minimize the extent of natural aging. The parent plate of AA6082 has a baseline hardness of 110 HV, which is consistent with its T6 (fully aged) condition. The minimum hardness is ~42 HV in this alloy. This is reached only at temperatures greater than 375 °C. In terms of realistic welding times, where peak temperatures are likely to be sustained for a matter of seconds, maximal softening occurs only at 525 °C

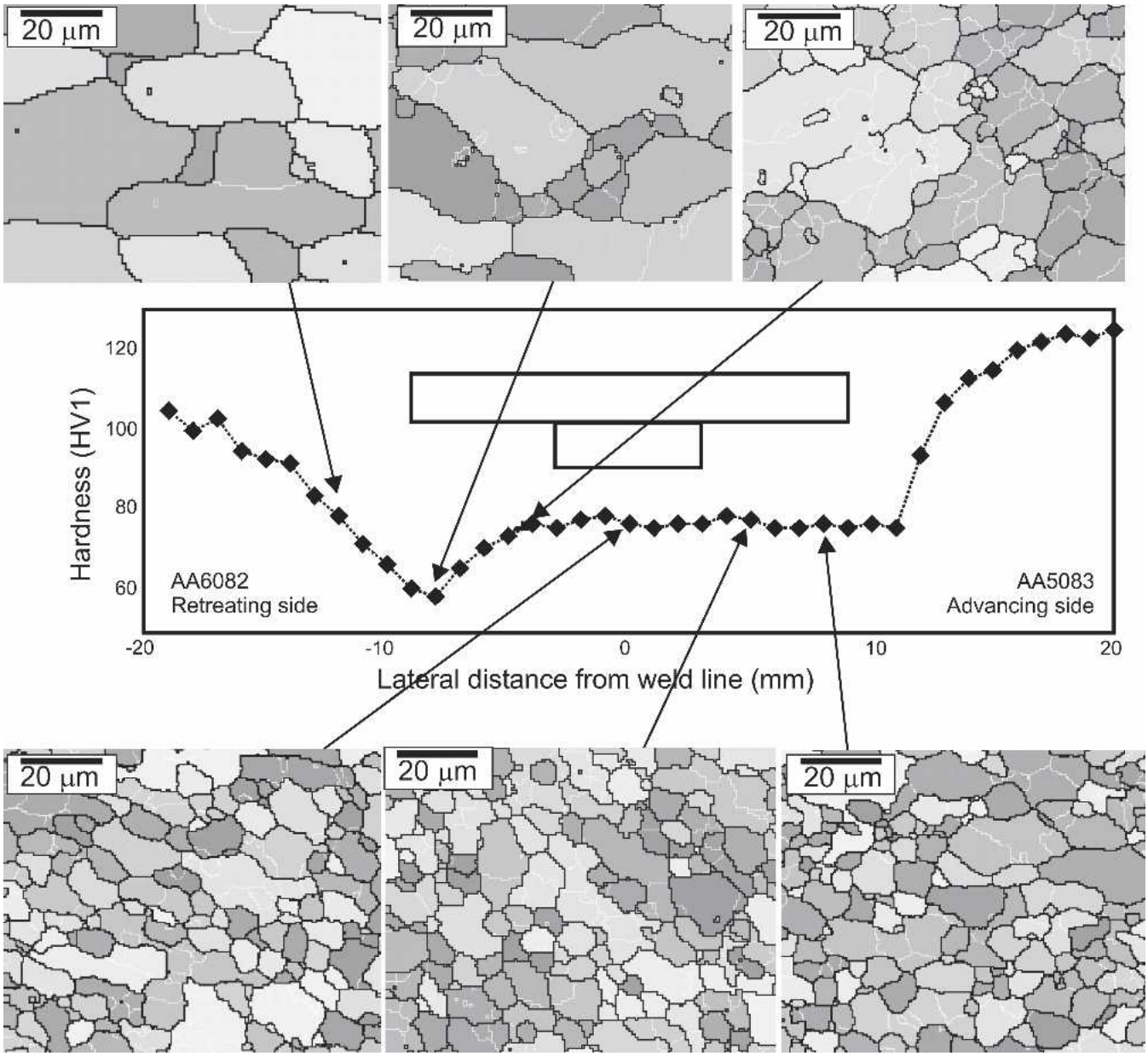

Fig. 4—EBSD maps taken close to the midthickness of the M5 weld showing the variation in grain structure (high-angle grain boundaries in black, low-angle in gray) in relation to the hardness profile in the weld. The region (bottom left) in the stir zone was selected to include only AA5083.

(in fact, the hardness is 50 HV at this temperature, probably as a result of some natural aging in the interval between quenching and testing). The extent of natural aging after 6 weeks of natural aging is presented in Figure 8(b). At this point aging is essentially complete, as most of the hardening occurs within 5 to 7 days. It can be seen that the level of natural aging is negligible in samples held at temperatures less than 375 °C. In contrast, at 525 °C the increase in hardness is constant, at 30 HV, indicating that dissolution is complete even at short hold times.

IV. ANALYSIS OF THE HARDNESS VARIATION ACROSS FS WELDS

Marked variations in hardness have been measured local to the FS welds in Figure 1. These variations determined the locations of failures in the cross-weld testing described in part I.[2] If it is not possible to restore the hardness by subsequent aging of the joint, then it will be necessary to design around the softer region and use appropriate safety factors. Consequently, it is important to understand the relationship between weld process condition, thermal history, and the resulting hardness. In this regard a simple, empirical model based on the predicted thermal history for estimating the hardness may be a useful tool. If successful, such a model would validate the thermal model on which it depends—particularly close to the tool, where thermocouple data are not available. Furthermore, it would provide a measure of the hardness of AA6082 immediately after welding before natural aging can occur and for which it is difficult to make actual measurements. Since the yield strength of the material during and immediately

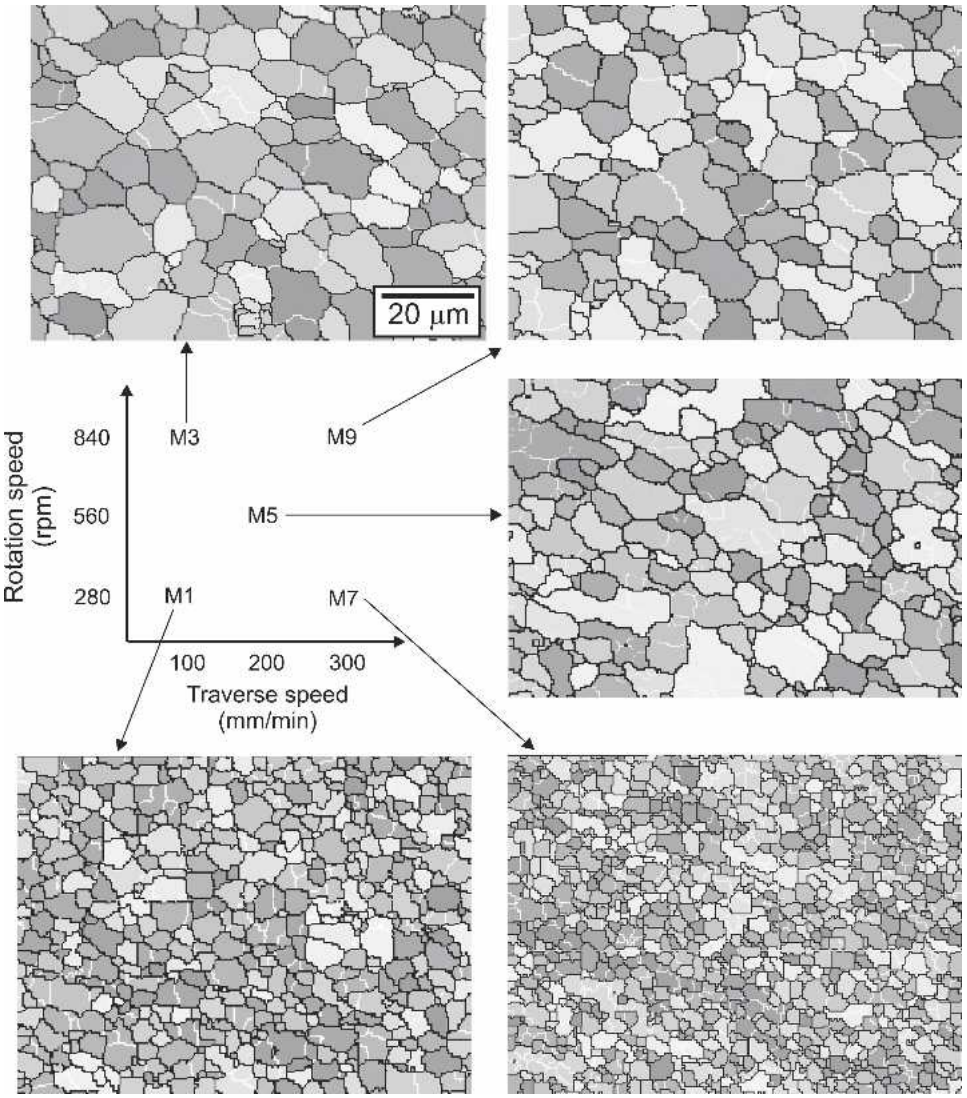

Fig. 5—EBSD maps of AA5083 material in the stir zone, at the intersection of the weld line and the midthickness of the plate, for welds produced under different conditions, each with AA5083 on the advancing side.

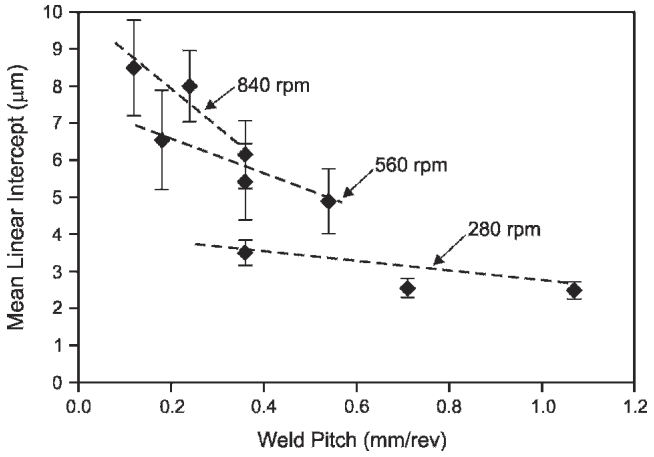

Fig. 6—A plot of the grain size in theAA5083 nugget region plotted against the weld pitch in welds M1–9 (AA5083 on the advancing side).

after welding can have a controlling effect on the residual stresses, a prediction of the instantaneous hardness is useful in assessing the capacity of the weld to sustain significant residual stresses. In the following section a model of hardness is presented, coupling the thermal model developed in part I on the basis of thermocouple results to a hardness model trained on classical isothermal measurements. As a result, a comparison with the FSW hardness curves represents a valid test of the thermal model.

A. *Modeling the Hardness of AA5083*

It has been shown that the softening of the AA5083 in the FS weld process zone is driven largely by the recrystallization and recovery of the cold-worked parent plate.[7] The rate at which these processes occur in a deformed material is dependent on the material condition (dislocation density, grain size, texture), the annealing temperature, the

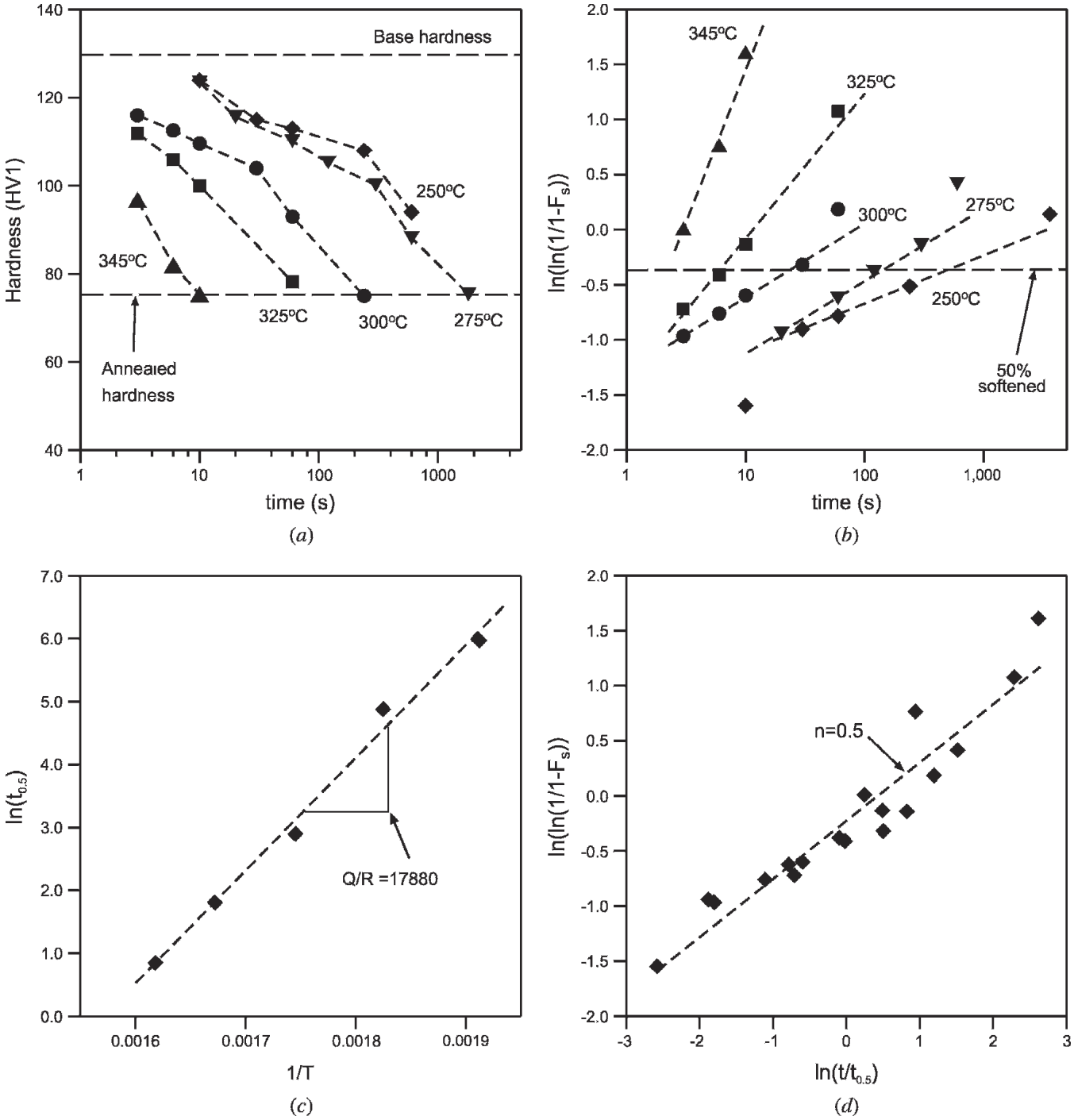

Fig. 7—(*a*) The hardness of AA5083 parent material after isothermal exposure at various temperatures and times (standard error is around 2 HV), (*b*) the recrystallized fraction estimated from the resulting hardness measurements as a function of isothermal hold time and temperature, (*c*) plot of $\ln(t_{0.5})$ against $1/T$ for the determination of Q_{soft}, (*d*) plot of $\ln(\ln(1/1 - F_s))$ against $\ln(t/t_{0.5})$ for the determination of the Avrami exponent.

rate of heating, and the structure/properties of the material in question.[18] A common approach to modeling the recrystallization of industrial aluminum alloys during isothermal heating is to use a modified version of the Johnson-Mehl-Avrami-Kolmogrov (JMAK) equation:[19–22]

$$X_v = 1 - \exp\left[-0.693\left(\frac{t}{t_{0.5}}\right)^n\right] \qquad [1]$$

where X_v = the fraction recrystallized, n = the Avrami exponent, and $t_{0.5}$ = the time required to reach 50 pct recrystallization. The value of $t_{0.5}$ for a given material, at a given temperature, is often estimated using an equation of the form:[23,24]

$$t_{0.5} = f(d_g, \varepsilon, Z)\exp\left(\frac{Q_{\text{rex}}}{RT_{\text{rex}}}\right) = A\exp\left(\frac{Q_{\text{rex}}}{RT_{\text{rex}}}\right) \qquad [2]$$

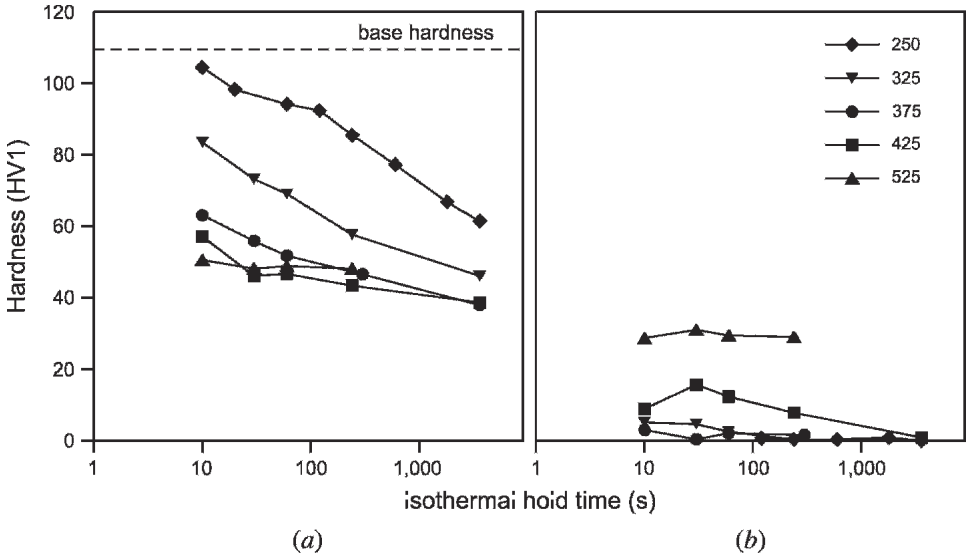

Fig. 8—(*a*) The effect of isothermal heat treatments on the hardness of AA6082. (*b*) The extent of natural aging represented as the difference between the hardness after quenching and after 6 weeks of natural aging. The estimated error is ±2 HV.

where ε = the previously applied strain, d_g = the original grain size, T_{rex} = the isothermal holding temperature, R = the universal gas constant, and Q_{rex} = the effective activation energy for recrystallization. Z is the temperature compensated strain rate given by the Zener-Hollomon parameter $Z = \dot{\varepsilon}\exp(Q_{def}/RT_{def})$ where $\dot{\varepsilon}$ is the strain rate, Q_{def} = the activation energy for deformation, and T_{def} = the deformation temperature. In the current case the deformation conditions of the parent plate are unknown and the same everywhere, and so the material-dependent parameters have been replaced by a single constant, A. The constants A and Q_{rex} can be estimated by regression from experimental data obtained from classical isothermal exposure tests.

The purpose of this model is to estimate the extent of softening of the AA5083 after welding rather than the fraction of recrystallized material. The relative softening can be determined from hardness indents by:[18]

$$F_s = 1 - \left(\frac{HV_{HT} - HV_{FS}}{HV_{FH} - HV_{FS}}\right) \quad [3]$$

where HV_{HT} = the hardness after heat treatment and HV_{FS} and HV_{FH} = the hardnesses of the fully softened and fully hard (*i.e.,* parent) material, respectively.

The determination of the constant A, the Avrami exponent n, and the activation energy for softening (Q_{soft}) from the isothermal hold data in Figure 7(a) involves several steps. If the softening behavior of the AA5083 alloy can be described using the JMAK equation (Eq. [1]), then in a plot of $\ln(\ln(1/1 - F_s))$ against $\log(t)$, the data from any given temperature will fall on a straight line. Such a plot is shown in Figure 7(b). It can be seen that most points do indeed fall on a straight line, with the exception of very short or very long times, particularly at the lower temperatures (<300 °C). The intercept of the data fit with $F_s = 0.5$ provides an experimental estimate of $t_{0.5}$ at each temperature. Note that only the linear sections of the plots were fitted.

Eq. [1] predicts that in a plot of $\ln(t_{0.5})$ against $1/T$ (Figure 7(c)), the gradient will be equal to Q/R, where R = the gas constant. The intercept of this plot will provide the constant A. Analysis of the data and rounding to the nearest KJ indicates that Q_{soft} = 148 KJmol^{-1} while $A = 5.5 \times 10^{-13}$. Including the nonlinear points was found to change Q_{soft} by up to 10 KJ. Raghunathan *et al.*[19] found that the activation energy for recrystallization was 186 KJmol^{-1} in hot-rolled AA5083. This discrepancy may reflect the fact that recovery is included in the present analysis, while the previous study directly determined the recrystallized fraction. However, differences in composition or previous thermomechanical treatments between the two materials cannot be ruled out.

Once the values for $t_{0.5}$ have been determined for each temperature, n can be estimated from the gradient of a plot of $\ln(\ln(1/1 - F_s))$ against the time normalized with respect to $t_{0.5}$.[21] These data are plotted in Figure 7(d). Although there is some scatter in the data, a best fit using a least squares approach indicates a gradient of ~0.5. This is lower than that normally expected for JMAK kinetics, where n is normally in the range 2 to 4,[19,21] which could be due to the use of total softening rather than recrystallized fraction. It is certainly inappropriate to draw any strong conclusions from this value.

Eqs. [1] to [3] provide us with the capacity to estimate the fractional softening of a sample that has been held at a constant temperature for a given time. However, we wish to determine the effect of a continuously varying thermal cycle rather than an isothermal hold. This can be achieved by determining the "effective time" of the thermal cycle. Essentially, the thermal cycle is split into a series of isothermal holds of duration δt_i and temperature T_i. The effective time t_{eff} of the entire thermal cycle is given by the sum of each incremental hold:[22,24]

$$t_{\text{eff}} = \sum_i \delta t_i \ \exp\left(\frac{-Q}{RT_i}\right) \quad [4]$$

The recrystallized fraction will then be given by:

$$X_v = 1 - \exp\left[-0.693\left(\frac{t_{\text{eff}}}{\text{A}}\right)^n\right] \quad [5]$$

Using these equations, it is possible to estimate the fractional softening in AA5083 for any given thermal cycle.

B. *Modeling the Hardness of AA6082*

Modeling the hardness of AA6082 is more difficult than for AA5083, as the model must also account for the increase in hardness that occurs around the weld line as a result of natural aging after welding. The model used in the current study was developed by Myhr and Grong with some modifications, as reported by Russel.[11,25] Only the most relevant details are presented below in as far as they are required to apply the model. Those interested in the details are referred to the literature.[3,11,12,26,27,28]

In the model, the particles in AA6082 are separated into two groups: hardening β'' and GP zones and nonhardening β' and β phases. It is assumed that softening occurs by the dissolution of the hardening precipitates, which begins at around 200 °C, increasing in extent with temperature until dissolution is complete. Upon cooling, some solute will precipitate as nonhardening phases, but any remaining solute will contribute toward hardening through natural aging via the precipitation of GP zones and β''. Thus, the model includes three main elements: the dissolution of the hardening phases, the potential for reprecipitation of nonhardening phases during cooling, and the extent of natural aging.

The dissolution of the hardening precipitates is dependent on both the temperature and the time spent at that temperature. The fraction of precipitate remaining after an isothermal hold of duration t at a temperature T is given by:[11]

$$\frac{f}{f_0} = 1 - \left(\frac{t}{t_1^*}\right)^n = \alpha_1 \quad [6]$$

where α_1 = the relative hardness of the material, n = a time exponent (assumed to be constant and equal to 0.5 for rods and needles), and t_1^* is the temperature-compensated time for the dissolution of hardening phases. This is the time required to achieve full dissolution at a temperature T compared to the time (t_{ref}) required for full dissolution at some reference temperature T_{ref}:[29]

$$t_1^* = t_{\text{ref}} \ \exp\left(\frac{Q_{\text{diss}}}{R}\left(\frac{1}{T} - \frac{1}{T_{\text{ref}}}\right)\right) \quad [7]$$

where Q_{diss} = an effective activation energy for precipitate dissolution that is refined from isothermal hardness data (see below). Rather than perform a detailed and lengthy microstructural examination, it is possible to estimate the fraction of remaining precipitate by using Eq. [3] and replacing F_s with f/f_0.[11]

Eq. [6] predicts that in a plot of $\log(1 - f/f_0)$ *vs* $\log(t/t_1^*)$ the data will form a straight line with a gradient of 0.5. In fact, as a result of the increase in solute around the precipitates as dissolution progresses, the data will actually fall on a curve, as shown in Figure 9. This indicates that the exponent n changes throughout the dissolution process, and hence models based on Eq. [6] will tend to overestimate the softening behavior. An alternative approach to using Eq. [6] directly is to use Figure 9 as a kind of ''master curve'' or look-up table where values for the fraction of precipitates are determined directly from the graph for any estimated value of (t/t_1^*) [25]

The equations shown enable one to predict the softening response during the isothermal treatment of AA6082. To apply them to a continuously varying thermal cycle, such as that experienced during welding, we can use a similar approach to that used for the AA5083 material. The thermal cycle is split up into a series of incremental isothermal holds of time t_i and temperature T_i. Thus t/t_1^* is replaced by the integral $\int_0^t dt/t_1^*$. This integral can be evaluated by summing the value of t/t_1^* for each incremental hold.[25] The fraction of precipitates remaining can then be determined from the master curve (Figure 9).

In the regions where dissolution occurs, and hence solute remains in the material, some precipitation of β'' and GP zones may occur, leading to recovery of some of the hardness. The maximum hardness after natural aging (approximately 80 HV) is significantly lower than the T6 condition due to the nonoptimal distribution and morphology of the precipitates and the reduction in available solute due to the precipitation of nonhardening β' during the cooling cycle.[14,30]

Myhr and Grong demonstrated that within the fully reverted region, the fraction of hardening precipitates can then be given by:[11]

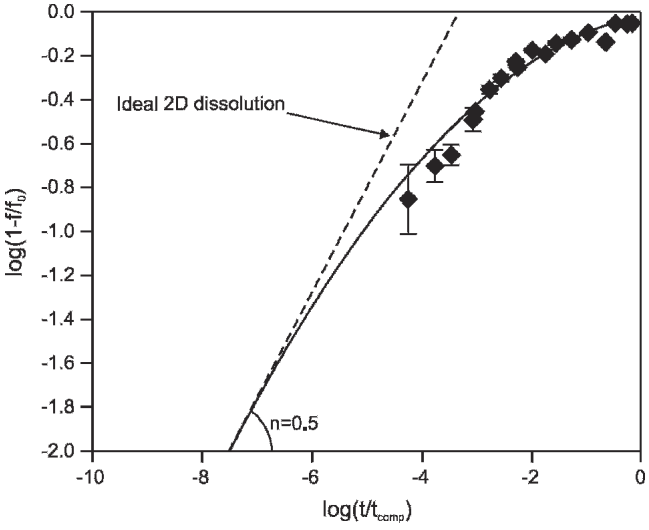

Fig. 9—The master curve for the softening of AA6082 estimated from the isothermal hold data in the current study. The curve is a best fit using an activation energy for dissolution of 190 KJ/mol. The straight line represents the ideal case of 2D dissolution in the absence of solute build-up in the surrounding matrix.

$$\alpha_2 = 0.56[0.95]^I \quad [8]$$

where the constant 0.56 = the relative hardness of the natural aged zone compared to the parent plate [*i.e.,* $(80-42)/(110-42)$]. I is the kinetic strength of the thermal cycle with respect to the precipitation of stable β phase:

$$I = \int_0^t \frac{dt}{t_2^*} \quad [9]$$

where t_2^* is the temperature compensated time to reduce α_2 to 95 pct of its original value at a temperature T, given by:

$$t_2^* = t_{r_2}^* \exp\left[\frac{A_0}{R}\left(\frac{1}{T(T_s-T)^2} - \frac{1}{T_{r_2}(T_s-T_{r_2})^2}\right) + \frac{Q_d}{R}\left(\frac{1}{T} - \frac{1}{T_{r_2}}\right)\right] \quad [10]$$

The parameters in this equation and the values used by Myhr and Grong (and here) are shown in Table I.

If the thermal exposure is insufficient to fully dissolve all of the precipitates, then Eq. [8] needs to be modified, and the most general equation for the natural aging after welding is obtained:[11]

$$\alpha_3 = 0.56\left[\left(\frac{\alpha_2}{0.56}\right)^{0.5} - \alpha_1\right] \quad [11]$$

where α_3 = the fraction of remaining precipitates after natural aging.

If the thermal cycle is known as a function of distance from the weld line, then the contributions by the softening and natural ageing models can be determined for each position using Eqs. [6] and [11]. The hardness at any point will be given by:

$$HV = HV_{\min} + (HV_{\max} - HV_{\min})\,\alpha_1 \quad \text{when } \alpha_1 \geq \alpha_3$$
$$HV = HV_{\min} + (HV_{\max} - HV_{\min})\,\alpha_3 \quad \text{when } \alpha_3 \geq \alpha_1 \quad [12]$$

The minimum hardness of the sample will be determined by the intersection of α_1 and α_3.

Although the material is nominally identical to that used by Myhr and Grong (*i.e.,* AA6082 in the T6 (fully aged) condition), it is prudent to check that our plate material follows the predicted behavior. This has been performed via a series of isothermal hold tests. The activation energy for the dissolution of the hardening precipitates has been determined using the method outlined by Russel and Shercliff.[29] In this method, the activation energy is adjusted in an iterative process until the data in a plot of $(1-f/f_0)$ versus $\log(t/t_1^*)$ falls on a continuous curve (if the activation energy is incorrect, those data will form several curves, one for each testing temperature). The data from the isothermal holds shown above are plotted in Figure 9. In general, the scatter in the data is fairly low, although it increases for samples with a low level of softening. This curve is essentially identical to that determined by Myhr and Grong.[11] The estimated effective activation energy for dissolution is 190 KJmol^{-1}, which is slightly higher than the values estimated by Russel for AA2014-T6 (155 KJmol^{-1}) and AA7010-T6 (165 KJmol^{-1}).[25] This may indicate that dissolution occurs less readily in this alloy compared to the higher-strength 2xxx and 7xxx series age-hardening alloys.

C. *The Predicted Weld Hardness*

Figure 10 shows the predicted variation in hardness across weld M9 (840 rpm and 300 mm/min) directly after welding, before natural aging can occur, and after natural aging is complete. While the hardness of the AA6082 close to the weld line is similar to that in the AA5083 when the weld is in the fully aged condition, in the as- welded condition the hardness is very different in the two alloys.

The hardness predicted by the models is compared to the experimental data in Figure 11. It can be seen that for the most part, the model is in good agreement with the experimental data. Specifically, the model is in good agreement with those welds where thermocouple data are available (M1, M3, and M9) but does not agree so well with the weld where actual temperature data are not available (M7). In this weld, the predicted width of the HAZ is slightly too wide, implying that the thermal model has overestimated the peak temperature and/or the length of the thermal cycle. The AA5083 softening model is somewhat more successful than the aging model for the AA6082. In the former case there is an encouraging level of agreement between the predicted and experimental data, including the similar hardness variations for the welds produced at the same weld pitch. The AA6082 model shows a good level of agreement only for weld M3, which has the widest HAZ. It is encouraging that the model accurately predicts the maximum hardness of the naturally aged region in all of the welds, but the point of minimum hardness is consistently too far from the weld line, apparently as result of an overestimation of the amount of dissolution. This may have occurred because the softening model is overly sensitive to the dissolution of the hardening phases or because the thermal model overestimates the temperature near the tool. It is known that the predicted temperature at 15- and 30-mm

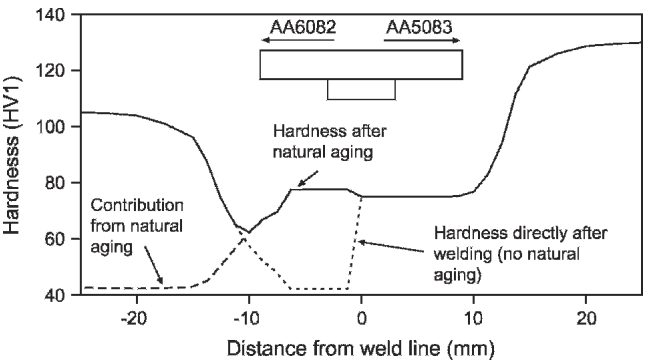

Fig. 10—The predicted variation in hardness across FS weld M9 (840 rpm and 300 mm/min) before and after natural aging based on the isothermal tests and the thermal history model.

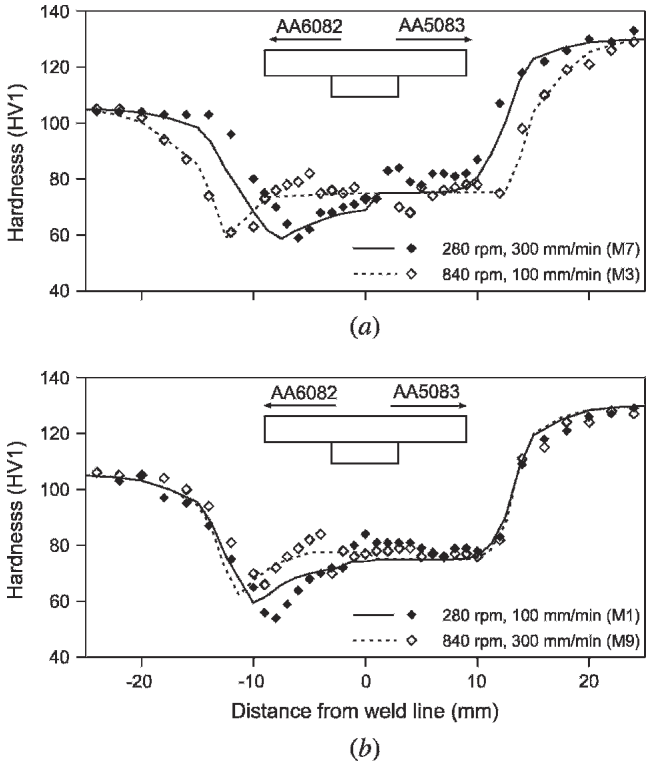

Fig. 11—A comparison of the predicted and measured hardness profiles in the dissimilar welds with AA5083 on the advancing side for (*a*) welds with the highest (1.1 mm/rev) and lowest (0.12 mm/rev) weld pitches and (*b*) welds with the same weld pitch (0.36 mm/rev).

distance is in good agreement with the experimental data (since the model was calibrated with these values), but it has not been determined whether the temperatures within 15 mm are representative of the actual conditions. Since the softening in the AA6082 occurs closer to the tool than the AA5083, the AA6082 model will be more sensitive to inaccuracies in the predicted temperature near the tool.

V. DISCUSSION AND SUMMARY

The aim of this paper has been to investigate the relationship between the welding speeds, rotation and traverse, and certain microstructurally related characteristics of dissimilar FS welds between AA5083 and AA6082. These include the hardness variation across the weld and the grain size and structure within the weld. The former has been further investigated by the implementation of two materials models that can predict the hardness as a function of distance from the weld line. These models use the predictions of the thermal model presented in part I.[2] The model can explain the hardness variations in both AA5083 and AA6082.

In part I[2] we concluded that the temperature close to the weld line was governed primarily by the rotation speed, while the traverse speed had a secondary influence. The variation in grain size in the AA5083 material and the extent of natural aging in the AA6082 would seem to support this conclusion. The hardness models provide a sterner test of the thermal model, as there must be a quantitative agreement between the real and predicted data. In general there is a reasonable agreement, in particular for the AA5083. The most significant discrepancy is in overestimating the distance of the point of minimum hardness from the weld line in the AA6082. This may be a result of inaccuracies in the thermal model due to the somewhat simplistic representation of the tool.[2]

The data from the current study would suggest that for this combination of materials, problems of under- or overheating during welding are best solved by changing the rotation speed rather than the traverse speed. Even large changes in the traverse speed may not significantly alter the temperature around the tool. It is also noteworthy that the extensive hardening of the AA6082 upon natural aging raises the hardness in the welding region to a value near that of the AA5083. However, the lower hardness, and hence strength, during and immediately after welding on this side of the weld may limit the magnitude of the residual stresses that can build up in this location.

ACKNOWLEDGMENTS

This work is part of the Brite-Euram project "Join-DMC" with project number GRD1-1999-10551. The authors thank Drs. J. Wert, T. Lorentzen (Risø), C. Dalle-Donne (DLR), and F. Palm (EADS). The technical assistance of Mr. I. Brough and Mr. P. Kenway is appreciated. P.J.W. acknowledges a Royal Society-Wolfson Merit award.

REFERENCES

1. W.M. Thomas, E.D. Nicholas, J.C. Needham, M.G. Murch, P. Temple-Smith, and C.J. Dawes: *Friction Stir Butt Welding*. 1991 International Patent No. PCT/GB92/02203.
2. M. Peel, A. Steuwer, P.J. Withers, T. Dickerson, Q. Shi, and H.R. Shercliff: *Metall. Mater. Trans. A.*, 2006, vol. 37A, pp. 2183-93.
3. Ø. Grong: *Metallurgical Modelling of Welding*. Materials Modelling Series, edited by H.K.D.H. Bhadeshia. Institute of Materials, 1994.
4. Y.S. Sato, H. Kokawa, M. Enomoto, and S. Jogan: *Metall. Mater. Trans.*, 1999, vol. 30, pp. 2429-37.
5. L.E. Svensson, L. Karlsson, H. Larsson, B. Karlsson, M. Fazzini, and J. Karlsson: *Sci. Technol. Weld. Joining*, 2000, vol. 5 (5), pp. 285-96.
6. H. Jin, S. Saimoto, M. Ball, and P.L. Threadgill: *Mater. Sci. Technol.*, 2001, vol. 17 (12), pp. 1605-14.
7. M. Peel, A. Steuwer, M. Preuss, and P.J. Withers: *Acta Mater.*, 2003, vol. 51 (16), pp. 4791-801.
8. F.J. Humphreys: *Vmap: Quantitative Metallography by Electron Backscattered Diffraction,* 2002.
9. F.J. Humphreys: *J. Mater. Sci.*, 2001, vol. 36 (16), pp. 3833-54.
10. S.B. Kang, L. Zhen, H.W. Kim, and S.T. Lee: *Mater. Sci. Forum*, 1996, vol. 217–222, pp. 827-32.
11. O.R. Myhr and Ø. Grong: *Acta Mater.*, 1991, vol. 39 (11), pp. 2693-702.
12. O.R. Myhr and Ø. Grong: *Acta Mater.*, 1991, vol. 39 (11), pp. 2703-08.
13. S.J. Andersen, H.W. Zandbergen, J. Jansen, C. Traeholt, U. Tundal, and O. Reiso: *Acta Mater.*, 1998, vol. 46 (9), pp. 3283-98.
14. A.K. Gupta, D.J. Lloyd, and S.A. Court: *Mater. Sci. Eng. A*, 2001, vol. 301 (2), pp. 140-46.
15. G.A. Edwards, K. Stiller, G.L. Dunlop, and M.J. Couper: *Acta Mater.*, 1998, vol. 46 (11), pp. 3893-904.
16. K.V. Jata and S.L. Semiatin: *Scripta Mater.*, 2000, vol. 43 (8), pp. 743-49.
17. C.G. Rhodes, M.W. Mahoney, W.H. Bingel, R.A. Spurling, and C.C. Bampton: *Scripta Metall.*, 1997, vol. 36, pp. 69-75.
18. F.J. Humphreys and M. Hatherly: *Recrystallization and Related Annealing Phenomena,* 3rd ed. Pergamon Press, 2002.
19. N. Raghunathan, M. Zaidi, and T. Sheppard: *Mater. Sci. Technol.*, 1986, vol. 2, pp. 938-45.
20. J. Go, W.J. Poole, M. Militzer, and M.A. Wells: *Mater. Sci. Technol.*, 2003, vol. 19 (10), pp. 1361-68.

21. T. Furu, H.R. Shercliff, G.J. Baxter, and C.M. Sellars: *Acta Mater.*, 1999, vol. 47 (8), pp. 2377-89.
22. I.V. Samarasekera, M.A. Wells, D. Jin, C.O. Hlady, J.K. Brimacombe, and E.B. Hawbolt: *Mater. Charact.*, 1995, vol. 35 (1), pp. 69-79.
23. N. Raghunathan, M. Zaidi, and T. Sheppard: *Mater. Sci. Technol.*, 1986, vol. 2, pp. 938-45.
24. T. Sheppard and X. Duan: *J. Mater. Process. Technol.*, 2002, vol. 130–131, pp. 250-53.
25. M.J. Russel: *Analytical Modelling of Friction Stir Welding*. University of Cambridge, 2000.
26. Ø. Grong and H.R. Shercliff: *Prog. Mater. Sci.*, 2002, vol. 47 (2), pp. 163-282.
27. B.I. Bjorneklett, Ø. Grong, O.R. Myhr, and A.O. Kluken: *Acta Mater.*, 1998, vol. 46 (17), pp. 6257-66.
28. D.H. Bratland, Ø. Grong, H. Shercliff, O.R. Myhr, and S. Tjotta: *Acta Mater.*, 1997, vol. 45 (1), pp. 1-22.
29. M.J. Russel and H.R. Shercliff: First International Symposium on FSW (CD-ROM), Thousand Oaks, CA, 1999.
30. J.L. Cavazos and R. Colas: *Mater. Charact.*, 2001, vol. 47 (3–4), pp. 175-79.